Journal of Field Robotics

WILEY

RESEARCH ARTICLE OPEN ACCESS

A Controllable-Stiffness Tensegrity Robot Joint for Robust Compliant Manipulation

Yifeng Hao[1] | Jing Dai[1] | Zhiyi Jiang[1] | Alex Pui-Wai Lee[2] | James Lam[1] | Ka-Wai Kwok[1,3]

[1]Department of Mechanical Engineering, The University of Hong Kong, Hong Kong, China | [2]Department of Medicine and Therapeutics, The Chinese University of Hong Kong, Hong Kong, China | [3]Department of Mechanical and Automation Engineering, The Chinese University of Hong Kong, Hong Kong, China

Correspondence: Ka-Wai Kwok (kwokkw@hku.hk)

Received: 1 July 2024 | **Revised:** 9 December 2024 | **Accepted:** 13 April 2025

Funding: This work is supported in part by the Research Grants Council of Hong Kong under Grant 17209021, 17210023, 17204124, STG1/E-401/23-N and C4026-21G; in part by the Multi-Scale Medical Robotics Center Ltd. funded by the Innovation and Technology Commission (ITC), Hong Kong; in part by the Guangdong Basic Research and Applied Basic Research Fund under Grant 2024A1515011509.

Keywords: compliant manipulation | controllable stiffness | hybrid control | tendon-driven actuation | tensegrity

ABSTRACT

With concerns about safety in human–robot interactions, there is a growing demand for *inherent* compliance in robot manipulation, especially in healthcare applications, where remote tendon-driven mechanisms have drawn increasing attention, as they can reduce the overall robot joint size and weight by decoupling the motor from the rotary joint via tendon transmission. However, tendon preloading or any external load on the robot links would still be the predominant cause of excessive friction at the joint, deteriorating overall efficiency of the remote mechanical transmission. Our recent work proposed a tensegrity structure as a tendon-driven parallel mechanism for robot joint actuation, in which rotary/sliding friction at the joint can be totally avoided. The stiffness of such tensional integrity structure could be controlled by just tightening the tendons in parallel. Herein, we intend to integrate both tendon force/tension sensors and primitive axial stiffness modulators along the tendons, to close the stiffness control loop by a feedback model that estimates statics-equilibrium stiffness. A stiffness controller is also proposed, which can be operated in hybrid feedback modes involving a model-based stiffness estimator and a data-driven compensator. The proposed control framework is validated in particular for robot-assisted ultrasound scanning. We demonstrate that, even using simple or primitive stiffness modulators integrated along the tensegrity tendons, the robot joint stiffness can be controlled steadily under synthesized dynamic disturbances. The proposed data-driven stiffness compensator could compensate for uncertainty in modeling the complex statics equilibrium of our tensegrity structure, ensuring high-fidelity stiffness control.

1 | Introduction

Robot assistants have been introduced to healthcare settings (Figure 1a) for collaborative manipulation (Oliveira et al. 2024), accredited to the advantages of flexibility and adaptability. Conventional collaborative manipulators generally feature rigid links, rotary joints, and force/torque sensors. Despite their precise and stable manipulation, the trade-offs in terms of large robot footprint and bulky weight still pose a high risk in human–robot interaction. This creates demand for inherent *compliance* in robot motion, particularly in healthcare applications such as interventional treatments, of which the requirements set a new benchmark for safe interaction.

High robot inertia or impulsive robot force are examples of risk in many interaction tasks where humans are closely involved.

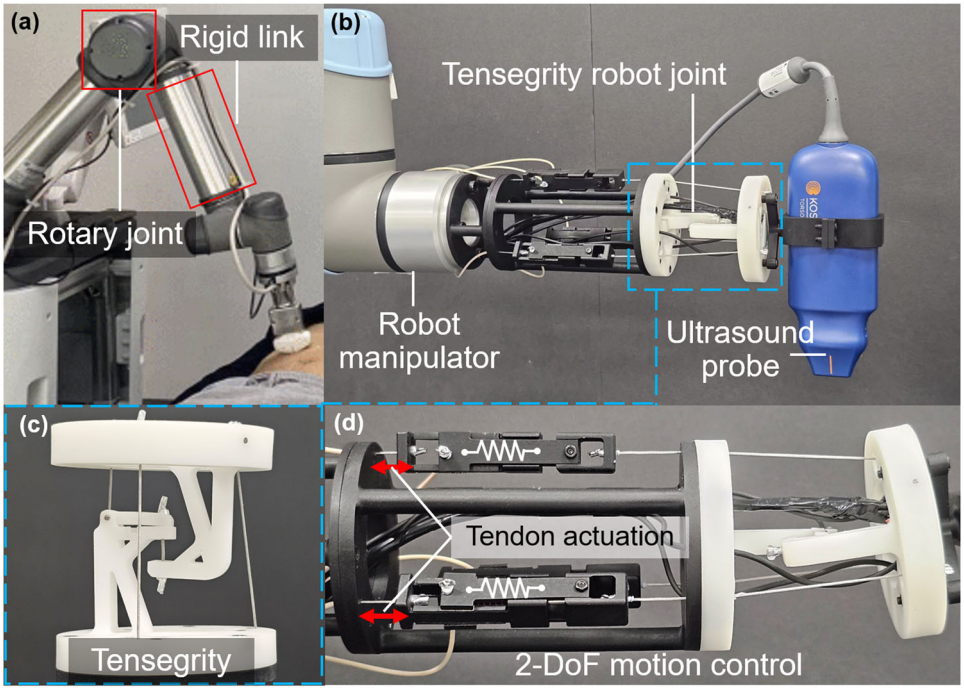

FIGURE 1 | (a) Example of conventional *rigid*-link and *rotary*-joint serial manipulator (i.e., UR5) performing collaborative ultrasound scanning (Image source: (Fu et al. 2023)). (b) *Soft* tensegrity robot joint extended from the UR5e robot. The joint inherits with inherent compliance for maneuvering an ultrasound probe. (c) Tensional integrity of a primitive tensegrity example, in which the structure is maintained by four tendon tensions. (d) 2-DoF motion, pan and tilt, that implemented by tendon contraction (red arrows). [Color figure can be viewed at wileyonlinelibrary.com]

To enhance robot compliance, incorporating multimodal sensors with sophisticated controllers is usually the primary option. Force/torque sensors seamlessly integrated at the robot joints become a standard setting, creating significant room for improvement in the aspect of control. Various control observers were developed previously to obtain a compliant response for collision detection. Model-based generalized momentum observers (GMO) (Luca et al. 2006; Luca and Mattone 2005) were typical examples to detect impulsive collision by computing the difference between the actual applied torque and the desired torque calculated from the dynamics model. Somehow, the uncertainty of the model would be a critical issue. Learning-based methods, for example, Long Short-Term Memory (Lim et al. 2021), were proposed to improve modeling reliability. However, the tuning of detection thresholds is still indeterministic, attributed to the highly varying dynamic characteristics of the controlled torques. In the case of simple and light robot joints without joint force/torque sensors, the joint torque could mostly be estimated from its robot joint kinematic variables or motor actuation current; however, errors induced by any measurement noise and delays would be inevitable using such kinds of estimation approaches (Haddadin et al. 2017). Even with the precise dynamics model, the localization of link contact/collision would be found unreliable. Apart from software aspects in terms of the controller, hardware improvements were mostly focused on the advancement of compact torque sensors (Kim et al. 2022; Seok et al. 2020), for example, capable of offering precise sensing with high-frequency and -resolution feedback, for which the sensing range and resolution are always trade-offs. The common downside is either increased complexity of joint alignments adversely affecting the overall robot kinematics desired or increased weight of joints that increases overall robot weight.

In regard to robot actuators specific for compliant manipulation, some attempts involved variable stiffness actuators (VSA) (Wolf et al. 2016) capable of modulating rotational stiffness in the actuator/motor. A common method is to simply attach linear springs to the actuator output shaft (Mengacci et al. 2021), allowing mechanical control of its rotational stiffness by tightening the springs. Another approach is to integrate clutches that could selectively trigger the spring coupling within the planetary gear transmission (Hussain et al. 2021). These actuators could offer a large output torque (50–100 N·m) with a wide stiffness range (0–100 N·m/rad) (Sun et al. 2022), enabling tunable output torque/force and mechanical compliance to respond the external disturbances. Again, such stiffness modulation mechanisms, despite being tailor-made for motor gearboxes, would still increase the robot joint weight and size. This necessitates a larger actuation force that typically requires actuators with more weight to be integrated inside the joint, ultimately leading to a higher risk in human–robot interaction due to the high inertia of the manipulator.

Several studies have endeavored to reduce the weight of VSAs (Sun et al. 2022); however, miniaturizing the VSA mechanism at the joint still remains challenging due to its complicated (pneumatic) coupling with springs. Therefore, research attention has shifted toward decoupling the motor from the robot joint via remote tendon transmission. The goal is to reduce the overall joint size and weight, while maintaining sufficient distal dexterity and force (Chen et al. 2022; Le et al. 2016; K. Wang

et al. 2023). Additionally, *axial* stiffness modulators could be integrated simply with the linear transmission medium, namely along the tendon. It is worth noting that a large variety of *axial* stiffness modulators are available, when compared to *rotary* types, owing to the wide range of linear springs with different rigidity and elasticity. Aside from springs, new types of linear actuators, such as McKibben artificial muscles (Li et al. 2020), can also have inherent stiffness variability. Advanced materials (Chen and Sakovsky 2023; Levine et al. 2022) were proposed to modulate electrostatics at low frequency (< 50 Hz), to program the mechanical stiffness (Diller et al. 2018; Hinchet and Shea 2020).

In many conventional tendon-driven mechanisms, preloading the tendon tension, or any external load applied to the robot link, would induce significant linear compression on the rotary joint where the robot links are hinged by their rotary shaft and bearing, thereby inducing unpredictable rotary friction at the joint. This would become a key factor in deteriorating the manipulation stiffness control. Our recent work (Hao et al. 2024) proposed tensional integrity, *tensegrity*, as a tendon-driven *parallel* mechanism for robot joint actuation, in which the rotary/sliding friction can be *totally* avoided by sustaining the robot links' connection with tendon tension only, without direct coupling or contact between the links. It is advantageous to control the tensegrity joint stiffness by just tightening the tendons in *parallel*. Through the formulation of the form-finding problem (Sabelhaus et al. 2020), both the kinematics and the statics equilibrium constraints must always be satisfied, known as fully constrained, during the tensegrity joint operation. Note that the kinematics modeling could be complicated by the non-closed-form correlation between task space and actuation space (Hao et al. 2024). Currently, most works focus either on locomotion robots (Chen and Jiang 2019; Liu et al. 2022; Vespignani et al. 2018) or compliant shape control of the entire serial-link robot configuration (Li et al. 2020; Liu et al. 2021; Jie Zhang et al. 2022), but very few (Hao et al. 2024) have reported precise tensegrity control for robot manipulation task.

To bypass the challenges of the form-finding problem and enhance the compliance of the tensegrity joint, a few studies have attempted to allow for spare tendon lengths that do not fully constrain the structure (Liu et al. 2021; Ramadoss et al. 2022; Zappetti et al. 2022), facing challenges such as the unpredictable joint motion under varying loads and limited payload. Similar to VSAs, elastic springs have been adopted to replace the tendons (Zhang et al. 2022) and integrated within the tensegrity joint to suppress free motion with a certain level of bending stiffness. Repeatable and controllable bending motion can be achieved by training the mapping between joint shape and corresponding tendon configurations (Zhang et al. 2022). Thin McKibben artificial muscles, composed of inner pneumatic bladders and exterior braided sleeves, have also been used as actuation tendons to enhance motion precision (Li et al. 2020). However, the joint stiffness can only be changed offline by replacing the springs or artificial muscle, and the interaction behavior is controlled in an open-loop manner due to the lack of stiffness/compliance sensing feedback. Self-contained joint stiffness sensing and online closed-loop stiffness control are still greatly needed to fulfill the requirements of various manipulation tasks.

In this paper, with the aim of further demonstrating the capability of the tensegrity joint's high-fidelity stiffness control, we propose to integrate both tendon force/tension sensors and axial stiffness modulators along the tendons, demonstrating the self-contained dynamics/compliance sensing and modeling. We also present how to close the joint stiffness control loop by using our proposed feedback model that estimates statics-equilibrium stiffness for control reference. The proposed controller can also operate with hybrid feedback modes involving not only a model-based stiffness estimator but one that is also data-driven and capable of learning and compensating for the uncertainty in modeling the complex statics equilibrium. The major work contributions are listed below:

1. Design of a soft tensegrity joint featuring inherent compliance, of which the stiffness control loop can be closed directly by linear force sensing in the robot joint, remotely from their actuators.
2. Design of a hybrid stiffness controller that combines model-based and data-driven methods for closed-loop stiffness control due to the complexity of robot kinematics and statics modeling.
3. Experimental validation of the tensegrity robot's dexterity, which would be the first of its kind with controllable stiffness. The optimal control bandwidth, stiffness range, and control robustness against disturbance are evaluated, in particular for the application of robot-assisted ultrasound.

2 | Tensegrity Joint With Controllable Stiffness

The proposed controllable-stiffness tensegrity joint is shown in Figure 1b. The basic working principles of the tensegrity (Figure 1c), such as its kinematics and 2 degree-of-freedom (DoF) joint motion control (Figure 1d), have been reported in our previous work (Hao et al. 2024). In this study, we intend to increase the outer diameter (OD) and length of the previous structure to 70 and 74 mm, respectively (Figure 2a), so as to enlarge its overall workspace. To enhance its stiffness control capability, we incorporate an axial stiffness modulator, together with joint pose and tendon tension sensing at the robot joint for sensory feedback. To close the stiffness control loop, a stiffness estimation method is proposed based on tensegrity statics equilibrium. Additionally, a stiffness controller is developed, together with hybrid feedback modes involving a model-based stiffness estimator and a data-driven compensator.

2.1 | Tendon Tension Sensing and Control

A tensegrity structure is maintained by tensions, with its stiffness solely determined by the magnitude of the tensions. Therefore, structural stiffness control could be intuitively achieved by integrating axial stiffness modulators. To validate our stiffness control framework, a simple component, that is, spring, was selected. An axial stiffness modulator mainly comprising a slider connected to the actuation motor, a guide shaft connected to the actuation tendon, and two clamping plates fixed on the guide shaft is designed and shown in

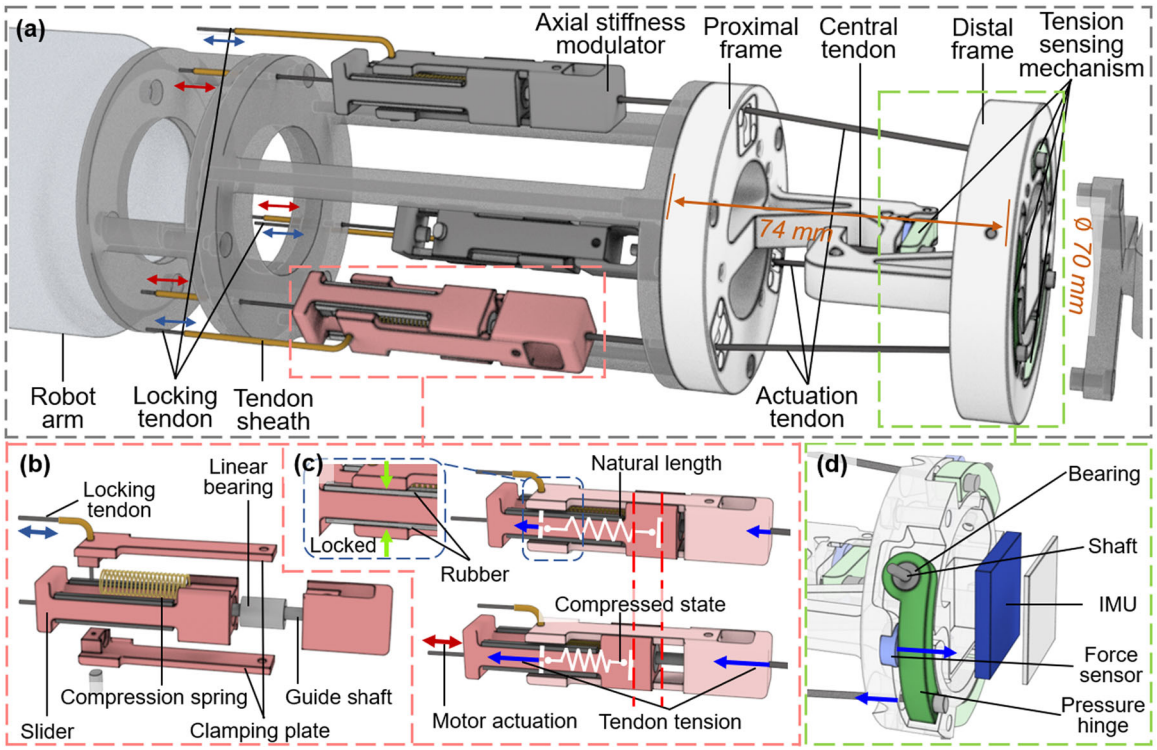

FIGURE 2 | Controllable stiffness feature of the proposed tensegrity robot joint. (a) Rendered graph showing the design details. The joint is fully constrained, while tension of the central tendon is the sum of the other three actuation tendons. Each actuation tendon is actuated by a motor outside the joint structure, allowing 2-DoF joint motion. (b) Exploded view of an axial stiffness modulator comprising a compression spring, which is compressed by the slider and two clamping plates fixed on the guide shaft. (c) Tendon tension modulation by compressing/restoring the spring inside. Spring compression could be locked by two clamping plates, the actuation of which can hinder the joint compliance as a whole. (d) Pressure hinge connected to the actuation tendon pulled onto a force sensor for tension sensing. An IMU is integrated into the distal frame, enabling self-contained sensing of the joint orientation. [Color figure can be viewed at wileyonlinelibrary.com]

Figure 2b. The slider and spring are concentrically placed through the guide shaft, with the spring being compressed by the slider and the clamping plates. Through motor actuation, the slider would be contracted and released, respectively, compressing and restoring the spring, thereby modulating the tendons' tension (Figure 2c). With increased tendon tension, higher structural stiffness would be achieved. Note that all the springs should be maintained in compression state during the compliant manipulation to ensure that the tensegrity structure still satisfies both kinematics and statics equilibriums, maintaining structural integrity by the tendons' tension.

Provided with the newly improved structure, reliable tension sensing feedback would be crucial for joint stiffness control. The actuation motors are mounted remotely from the robot joint to reduce joint weight and size, thus reducing the overall manipulation inertia. The total weight of the joint is only 180 g, including the stiffness modulators and cylinder supports. Despite its lightweight and compact design, it still provides 2-DoF manipulation, compared to the conventional rotary joint, which only provides 1-DoF rotation. However, the friction between the tendons and their pathway (e.g., tendon sheath; Figure 2a) would deteriorate tension sensing at the actuation end. To bypass the challenges in deducing the complicated friction model (Daemi et al. 2023; Li et al. 2024), a compact tension (force) sensing sensor is integrated inside the robot joint (Figure 2d). To sense the tension, one end of each tendon is mounted on a pressure hinge, which rotates about the shaft fixed on the joint distal frame. Tightening the tendon would pull the pressure hinge onto a force sensor (DYHW-108-H3.5, Dayang sensing), allowing tension changes to be measured with proper resolution by a leverage mechanism. Each force sensor is calibrated on a one-off basis so as to obtain an accurate leverage ratio. Such tension sensing can offer sensory feedback for the presented closed-loop stiffness control.

2.2 | Statics-Equilibrium-Based Stiffness Estimation Feedback

Given the self-contained sensory feedback of joint pose and tendon tensions, a model-based joint stiffness estimator is proposed and designed for closed-loop stiffness control. The stiffness $\hat{K}$ can be calculated by the applied force $\mathbf{F}_e \in \mathbb{R}^{3\times1}$ and joint end-effector position $\mathbf{z} \in \mathbb{R}^{3\times1}$:

$$\hat{K} = \frac{|\triangle \mathbf{F}_e|}{|\triangle \mathbf{z}|}, \tag{1}$$

where $\triangle$ denotes the changes in values.

As the structure integrity is maintained by tension, any disturbance would be passively distributed through the network of

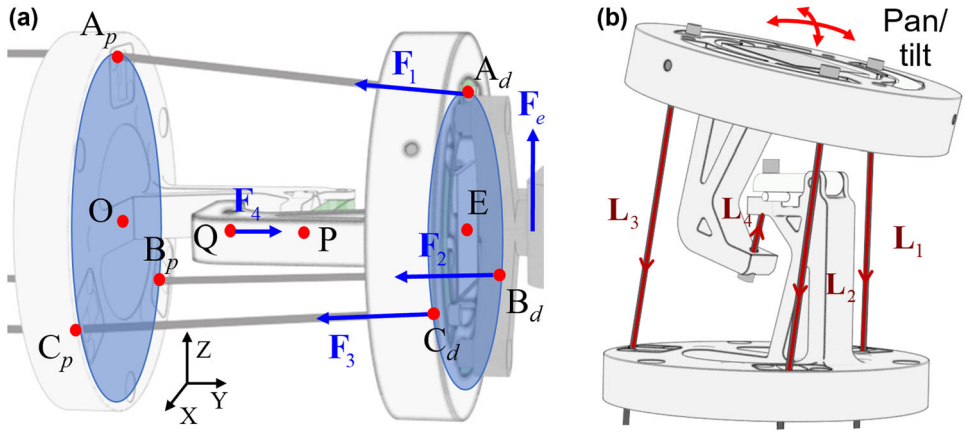

FIGURE 3 | Key parameters defined to deduce the tensegrity statics equilibrium. (a) Summation of internal forces $\mathbf{F}_i$, $i \in \{1, 2, 3, 4\}$ compensated by external force $\mathbf{F}_e$ under the statics equilibrium. (b) 2-DoF pan-tilt controlled by the lengths of three actuation tendon vectors $\mathbf{L}_1$, $\mathbf{L}_2$, and $\mathbf{L}_3$. [Color figure can be viewed at wileyonlinelibrary.com]

tension, such that the tendon tensions should have strong cues for estimation of the applied force. Regarding the joint distal frame (Figure 3a), the statics equilibrium can be expressed as

$$\sum_{i=1}^{4} \mathbf{F}_i = -\mathbf{F}_e, \tag{2}$$

where $i \in \{1, 2, 3, 4\}$ is the tendon index, and $\mathbf{F}_i = \left[F_i^x, F_i^y, F_i^z\right]^{\mathrm{T}} \in \mathbb{R}^{3\times1}$ is the tension applied by corresponding tendon $\mathbf{L}_i = \left[L_i^x, L_i^y, L_i^z\right]^{\mathrm{T}} \in \mathbb{R}^{3\times1}$. As the tendons are flexible, the force can be transmitted only through the tendon's axial direction, such that $\mathbf{F}_i$ and $\mathbf{L}_i$ are parallel. The force measured by 1-D force sensors is defined as $\mathbf{F}_t = [|\mathbf{F}_1|, |\mathbf{F}_2|, |\mathbf{F}_3|, |\mathbf{F}_4|]^{\mathrm{T}} \in \mathbb{R}^{4\times1}$. Assuming the tendon configuration $\mathbf{L} = [\mathbf{L}_1, \mathbf{L}_2, \mathbf{L}_3, \mathbf{L}_4] \in \mathbb{R}^{3\times4}$ can be obtained, then, Equation (3) can be represented by

$$\left[\frac{\mathbf{L}_1}{|\mathbf{L}_1|}, \frac{\mathbf{L}_2}{|\mathbf{L}_2|}, \frac{\mathbf{L}_3}{|\mathbf{L}_3|}, \frac{\mathbf{L}_4}{|\mathbf{L}_4|}\right] \times \mathbf{F}_t = -\hat{\mathbf{F}}_e, \tag{3}$$

where $\times$ denotes matrix multiplication and $\widehat{\mathbf{F}_e}$ is the estimated force. Therefore, $\widehat{\mathbf{F}_e}$ could be calculated, given the tendon tension $\mathbf{F}_t$ and the tendon configuration $\mathbf{L}$.

In general, the tendon configuration $\mathbf{L}$ could be calculated by joint kinematics model with tendon actuation $\mathbf{q} = [|\mathbf{L}_1|, |\mathbf{L}_2|, |\mathbf{L}_3|]^{\mathrm{T}}$ obtained from motor encoders, but the tensegrity kinematics modeling would be rather complicated. The joint distal frame is actuated in a complex swinging motion, which must also satisfy the boundary conditions decided by static equilibriums, leading to a non-closed form correlation between task space and actuation space (Hao et al. 2024). Alternatively, with the proximal frame's fixed position, the tendon configuration can be estimated with distal frame's 6-D pose and its geometry model. Previously, we implemented Fiber Bragg grating (FBG)-based sensing (Hao et al. 2024; Wang et al. 2021; Wang et al. 2020), which can provide self-contained shape sensing feedback for position control. However, not only the external force but also the varying pretension would stretch the strain sensor, thus deteriorating the sensing reliability. In this study, we integrate an inertial measurement unit (IMU, HFI-A9, Taobotics) into the joint (Figure 2d), which could provide precise joint orientation, namely the rotation $\mathbf{R} \in \mathbb{R}^{3\times1}$(represented as Euler angle). When the tensegrity is in both kinematics and static equilibriums, which is guaranteed by tendon pretension, there would be a unique mapping $\mathbf{z} = g(\mathbf{R})$ between joint orientation $\mathbf{R}$ and end-effector position $\mathbf{z}$. However, such mapping would be nonlinear and high-dimensional due to the abovementioned non-closed form correlation between joint task and actuation space. Therefore, a neural network (NN) model is employed to train the mapping $\mathbf{z} = g(\mathbf{R})$. It consists of ten hidden layers, and each layer contains 100 neurons. Regarding data collection, a two-step sampling method (Hao et al. 2024) was introduced to resolve the typical challenge in meeting the abovementioned equilibriums. Initial actuation sequences were first generated by a basic geometric model and then corrected in a torque-control manner by multiple trials of releasing and pulling the tendon individually. The ultrasound holder (Figure 1b) acts as the end-effector, whose positions $\mathbf{z}$ were recorded by an electromagnetic (EM) tracking system (NDI Medical Aurora), while the joint orientations $\mathbf{R}$ were recorded by the integrated IMU (Figure 2d). In this sampling method, there were 1953 data pairs collected for model training. Besides, the clamping plates (Figure 2c) should remain actuated and lock the spring compression, thereby making the joint compliance ineffective during the sampling. As the joint frames are rigid, the position of tendon fixations $\mathbf{A}_d$, $\mathbf{B}_d$, $\mathbf{C}_d$, and $\mathbf{Q}$ on the distal frame would remain unchanged relative to the ultrasound holder (Figure 3a). Given the instantaneous holder orientation $\mathbf{R}$ and position $\mathbf{z} = g(\mathbf{R})$ obtained by IMU, the positions of these fixations could be easily determined based on the frame geometry. As the positions of tendon pathway locations $\mathbf{A}_p$, $\mathbf{B}_p$, $\mathbf{C}_p$, and fixation $\mathbf{P}$ on the proximal frame remain unchanged in the joint base coordinate, the tendon configuration $\mathbf{L}$, which comprises the four tendon vectors, can be estimated with the two ends of the tendon known. Upon Equations (1) and (3), the joint stiffness $\hat{K}$ can also be estimated, thus offering feedback for closed-loop stiffness control (Figure 4).

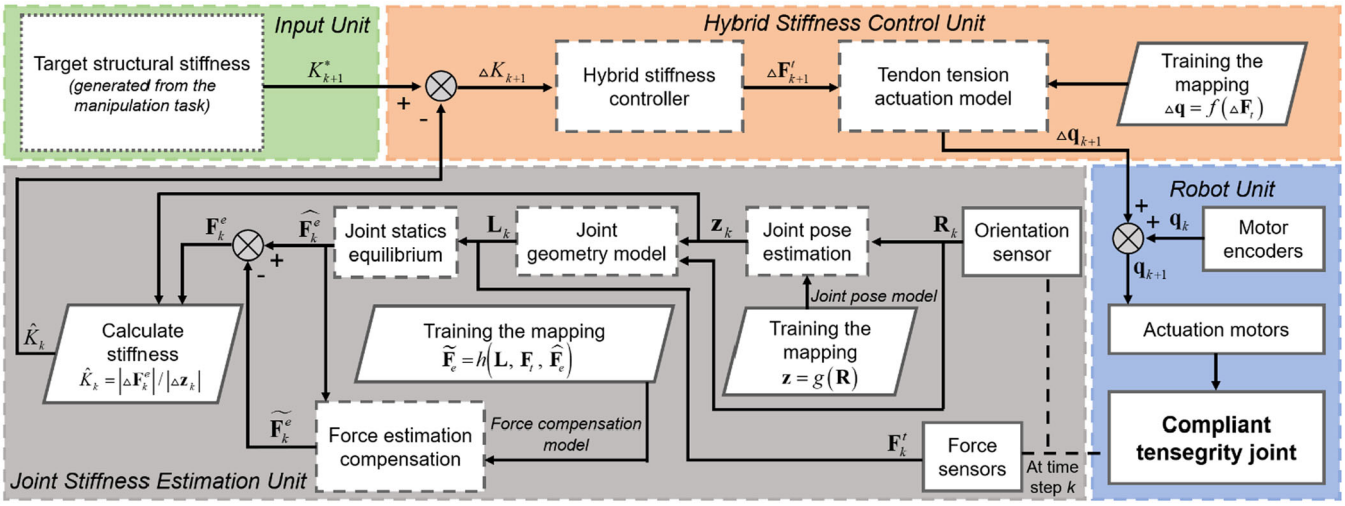

FIGURE 4 | Overview of the proposed stiffness control framework. A stiffness controller is implemented with hybrid feedback modes involving a model-based stiffness estimator and a data-driven compensator. Tendon tension $\mathbf{F}_t$ and joint orientation $\mathbf{R}$ are measured by force sensors and an orientation sensor (i.e., IMU), respectively. Provided with sensory information, joint stiffness $\hat{K}$ is estimated by the model-based estimator and calibrated by the data-driven compensator $h(.)$. [Color figure can be viewed at wileyonlinelibrary.com]

2.3 | Hybrid Closed-Loop Stiffness Control

Given the model-based stiffness estimator in Section 2.2, the stiffness control loop could be closed to respond to external disturbance. The estimator reliability could be further improved by compensating modeling uncertainty in complex statics equilibrium (Fang et al. 2019; Mak et al. 2024; X. Wang et al. 2023). Here, we intend to propose a data-driven compensation strategy to calibrate the applied force estimation in Equation (3) so as to investigate whether stiffness control robustness can be further enhanced. To collect data set, static loads ranging from 0.5 to 5 N were applied to the joint end-effector. Eight directions were selected, which are evenly distributed in the plane parallel to the joint frame. The applied force estimated by joint statics equilibrium was recorded and collected for the compensator training. An NN model consisting of ten hidden layers (100 neurons per layer) was established to train the compensator $\widetilde{\mathbf{F}}_e = h(\mathbf{L}, \mathbf{F}_t, \widehat{\mathbf{F}}_e)$. Given the learned compensator, the applied force in stiffness estimation can be calculated as

$$\mathbf{F}_e = \hat{\mathbf{F}}_e + \widetilde{\mathbf{F}}_e. \tag{4}$$

To control the joint stiffness, a controller that can be run in hybrid feedback modes involving the proposed model-based stiffness estimator and the data-driven compensator $h(.)$ is developed. The schematic diagram of the proposed stiffness control framework is shown in Figure 4. A joint stiffness model is another prerequisite in such control, while deducing the model from tensegrity statics could be challenging, due to the presence of complex motion generated and geometry constraints induced by kinematics equilibrium. Although there have been several works proposed with numerical constrained optimization methods, for example, force density method (Zhang and Ohsaki 2006) and dynamic relaxation (Bel Hadj Ali et al. 2011), the formulation of accurate model with effective optimization is still very complicated. Therefore, we intend to employ data-driven methods, where the stiffness model is deduced by the mapping between the tendon tensions and joint stiffness. To learn such mapping, the joint stiffness was evaluated through a load-deflection test (Section 3.1), in which the joint distal frame was moved upward by 5 mm using a UR5e manipulator (Universal Robots), while the applied forces were being recorded to calculate the stiffness. The stiffness was evaluated under four levels of tendon tension, 3, 6, 9, and 12 N. For each tension setting, the tests were repeated three times. The resultant force-deflection curves can be used to deduce joint stiffness model using linear regression.

3 | Experiment Results and Discussion

In this study, we focus on a new design of a high-order structural stiffness control framework, rather than relying solely on a positional controller as presented in our previous study (Hao et al. 2024). Among the various options for axial stiffness modulators that could be integrated with our tensegrity joint, we chose a simple implementation of springs to validate our stiffness control framework, which could potentially be applied to similar tensegrity structures with controllable stiffness features. The optimal control frequency was analyzed through frequency response experiments, and a data-driven stiffness model was derived from a load-deflection test. To evaluate the control performance and robustness of the hybrid stiffness control, we conducted experiments with dynamic disturbances and compared the control performance with and without learning-based compensation in stiffness estimation feedback.

3.1 | Joint Controllable Stiffness Under Static Load

Since rapid response can be a prerequisite for robust adjustment of joint stiffness, a frequency response test was conducted for the proposed robot joint. A small pretension of 2 N was applied to each actuation tendon to ensure that the tensegrity structure

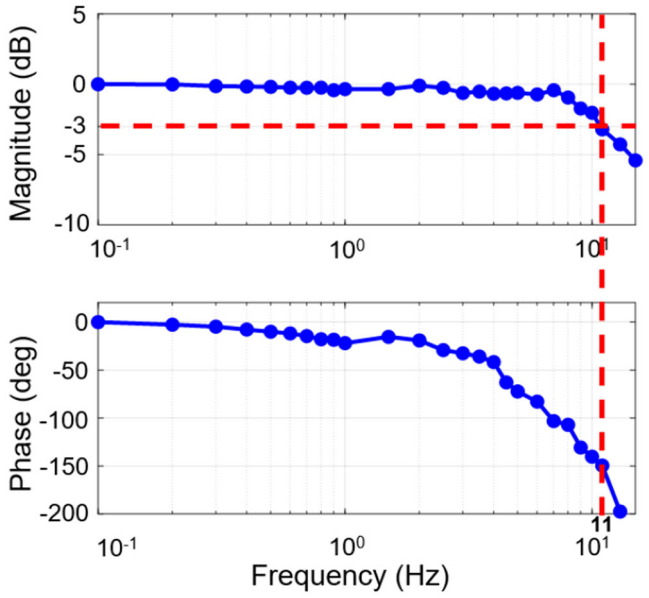

FIGURE 5 | Experimental frequency response of the present tensegrity operated with frequencies increased from 0.1 to 15 Hz. The bandwidth reaches about 11 Hz, where the magnitude decays by 3 dB. [Color figure can be viewed at wileyonlinelibrary.com]

would satisfy both kinematics and statics equilibriums. Two of the motors were commanded to produce periodic actuation that simultaneously pulls and releases the corresponding actuation tendons at frequencies ranging from 0.1 to 15 Hz. To enhance spatial resolution, the distal tip of the tensegrity joint was extended by 100 mm, and its position was measured by the EM tracking system. The resultant Bode plot, shown in Figure 5, indicates a cutoff bandwidth of 11 Hz. Such a cutoff frequency outperforms that in our previous tensegrity joint (Hao et al. 2024), attributed to the tendon pretension and the linear spring in the integrated stiffness modulator. When it comes to the major task in this study, that is, stiffness control, even with such improved positional response, the optimal control bandwidth would have to be determined by taking into account other concerns, in particular the frequency of the sensing feedback and the stiffness modulation. High tension would be applied to enhance structural stiffness, but it would inevitably induce large friction between tendon and its pathways (i.e., tendon sheath and tendon hole), even with pulleys and bearings at the joint frame intended to guide tendon actuation. High static friction would occur when the joint is forced to move by a disturbance and could induce impulsive noise in force sensing, thus deteriorating the control at high frequency. In terms of this stiffness modulation issue, our primitive tension modulator, which is integrated with springs, has a low modulation speed as it requires the motor actuation to compress and release the spring. The optimal stiffness control bandwidth should be determined based on the specific operation scenario, instead of only considering the tested positional response, so as to balance the trade-off between fast response to disturbances and sufficient time for stiffness modulation and robust sensing feedback. When specifically applied to the robot-assisted ultrasound scanning scenario in this study, the manipulation disturbances would be mainly induced by patient's respiration motion with a frequency at around 0.25 Hz (Ipsen et al. 2021; Thomas et al. 2021). Therefore, we kept the joint control at a bandwidth of 2 Hz during robot active manipulation to appropriately respond to the patient's motion. Potential improvement could be the integration of advanced axial stiffness modulators with faster modulation.

Considering the complexity of the tensegrity statics model, we employed a data-driven method to deduce the mapping from tendon tension to joint structural stiffness. The joint stiffness under four levels of tendon tension was evaluated, that is, 3, 6, 9, and 12 N. Regarding each tension setting, the UR5e moved the joint frame upward by 5 mm while recording the applied force (Figure 6a). The tests under each tendon tension setting were repeated three times for reliable evaluation. As shown in Figure 6b, the force-deflection relationship under each tension setting is nonlinear, with the slope changing with respect to deflection. The possible reason for this behavior could be that the joint's actual bending motion was generated by the swing motion of the joint distal frame about the proximal frame's apex (point **P** in Figure 3b), resulting in a complex force-deflection relationship described by the tensegrity statics model. To simplify the complex model for closed-loop stiffness control (as discussed in Section 3.2), we could assume that joint stiffness is consistent with small deflection, that is, the applied force is linear with deflection, and such modeling error induced would

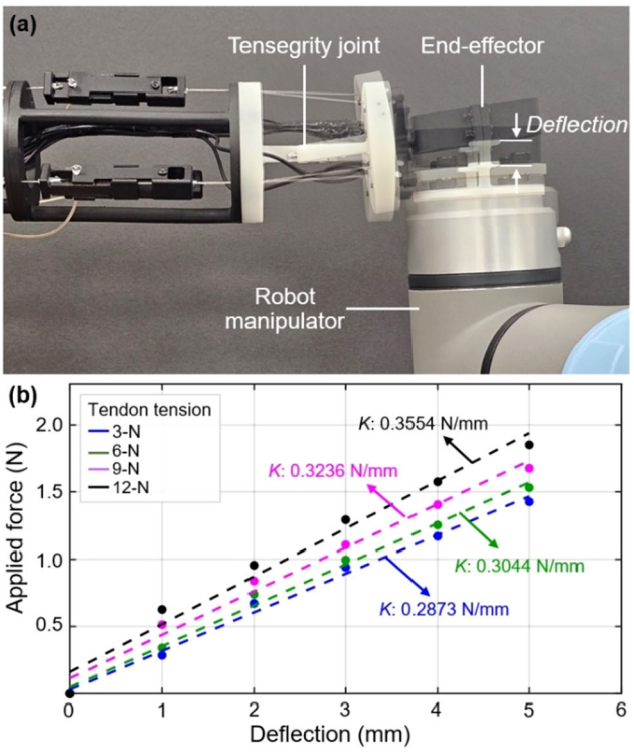

FIGURE 6 | Evaluation on joint stiffness under varied tendon tension. (a) Repeated disturbance force applied on the joint end-effector using a robot manipulator (UR5e). Measured deflection and forces of the joint determine stiffness under each tension setting. The joint end-effector was moved upward by UR5e within 1 to 5 mm. (b) Tendon tension ranged from 3 to 12 N. The linearity between deflection and applied force is derived by linear fitting using least-squares regression, in which the slope is defined as stiffness K. [Color figure can be viewed at wileyonlinelibrary.com]

be compensated by accurate joint stiffness feedback through the data-driven compensator $h(.)$. Therefore, we derived the linearity between the applied force and deflection by linear fitting using the least-squares regression, in which the slope was defined as the joint stiffness K. With the tendon tensions increasing from 3 to 12 N, the joint stiffness changed from 0.2873 to 0.3554 N/mm, accordingly. This indicates that joint structural stiffness can be readily adjusted by controlling the tensions. Based on the measured data, a data-driven joint stiffness model was deduced using linear regression, with stiffness as *input* and corresponding tendon tensions as *output*. Note that the above varied stiffnesses are under the regular condition, that is, the axial stiffness modulator is not locked by the clamping plates. When the compression of the spring integrated is locked, the structure could be fully constrained, and its compliance could be ineffective. Consequently, the tensegrity joint would achieve a high strength, for example, capable of lifting and shaking an object weighing 360 g with rapid changes in motion directions (Hao et al. 2024).

3.2 | Dynamic Stiffness Control

To evaluate the robustness of the proposed hybrid control against dynamic disturbances, stiffness control experiments were conducted under two conditions: ① stiffness feedback directly estimated from the model-based estimator and ② stiffness feedback with a data-driven compensator. Robot-assisted ultrasound abdominal scanning was selected as our objective scenario, where the stiffness control performance could be validated under disturbances induced by respiration motion. To simulate the disturbances, periodic displacements in the vertical direction were applied to the joint frame by the UR5e manipulator (Figure 6a). The motion frequency was set at 0.25 Hz, with an amplitude ranging from 0 to 8 mm, based on adult respiration motion patterns (Ipsen et al. 2021; Thomas et al. 2021) (see Video SV1). The optimal contact force for abdominal scanning could vary significantly depending on the specific task (Raina et al. 2021; Virga et al. 2016). Taking regular obstetric diagnosis as a test case, the average scanning contact force ranges from 4.28 to 9.05 N (Ulrich and Andreasen Struijk 2021). It is assumed that the contact force could be maintained below 6 N during the 0–8 mm respiratory motion. Considering the self-weight of the ultrasound probe (Torso-One, KOSMOS, USA) and the joint (~3.5 N), the experiment objective is to sequentially control the stiffness of the tensegrity joint toward four target values around 0.31, that is, 0.28, 0.30, 0.32, and 0.34 N/mm, without any pauses. As the joint initial condition before the tests, all actuation tendons were preloaded with 2 N. Three cycles of periodic displacement (12 s in total) were evaluated for each target (Figures 7a, 8a). The collected data (i.e., displacement and applied force) of the first half cycle were used to calculate the joint stiffness using Equation (1) as the ground truth.

The stiffness control results under condition ① are shown in Figure 7b. Across the four levels of target stiffness (0.28–0.32 N/mm), the actual joint stiffness was controlled from 0.2510 to 0.3021 N/mm, with rather constant errors from 0.0290 to 0.0379 N/mm. This discrepancy may stem from the inaccurate stiffness feedback due to the uncertainty in tensegrity statics. Within the joint statics equilibrium, the central tendon would have to afford the highest tension to balance the other three tendons' tension and external forces (Figure 3a). Therefore,

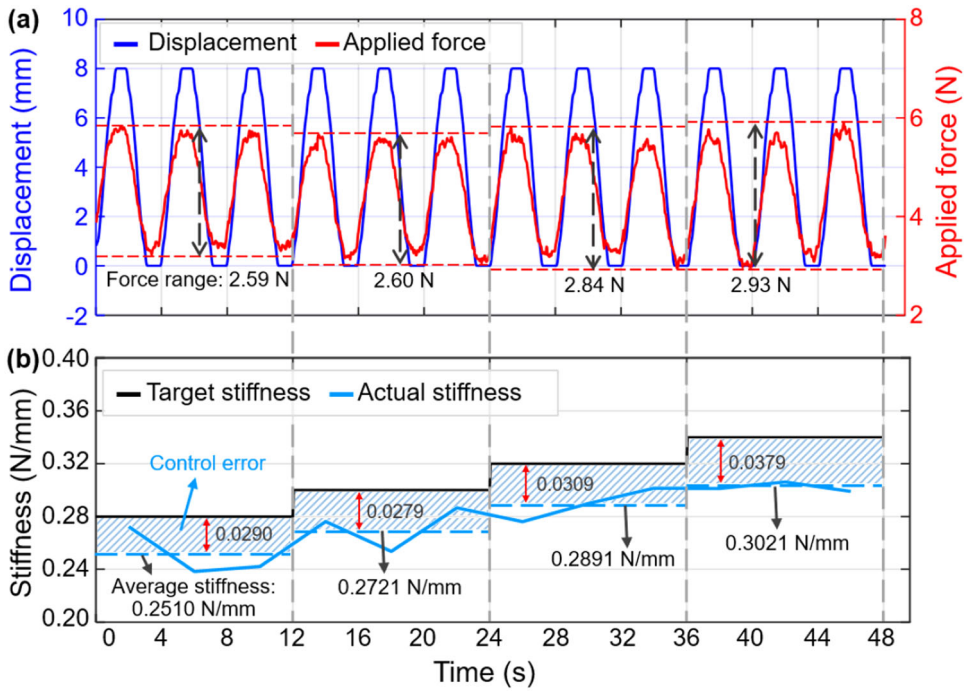

FIGURE 7 | Stiffness control with feedback from the model-based stiffness estimator only. (a) Force disturbance applied to the joint frame by the UR5e manipulator. The frequency and amplitude are, respectively, 0.25 Hz and 8 mm. To measure the actual joint stiffness, the applied force during displacement was recorded. (b) Controlled stiffness under four stiffness targets. The RMSE of control outcome is 0.0337 N/mm due to the inaccurate feedback. [Color figure can be viewed at wileyonlinelibrary.com]

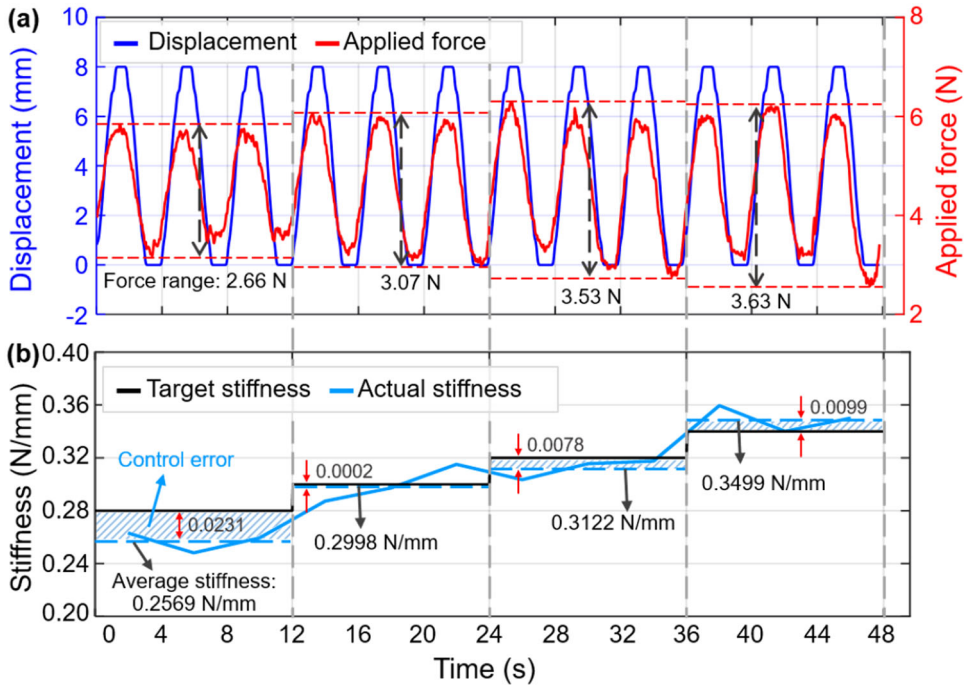

FIGURE 8 | Stiffness control with hybrid feedback, involving the model-based stiffness estimator and the data-driven compensator. (a) Same kind of dynamic disturbance of periodic displacement as in Figure 7. (b) Stiffness control outcome, such that the RMSE can reach 0.0156 N/mm, which is reduced by 53.7%, as compared to the test (Figure 7) without compensation. [Color figure can be viewed at wileyonlinelibrary.com]

braided steel tendon (OD 1.2 mm) is integrated to ensure the central tendon's rigidity and strength, avoiding significant elongation generated during joint motion. Additionally, the central tendon is designed to have a limited length (Figure 3b) so as to allow sufficient bending angles ($\pm 20°$) without collisions between the two joint frames. Under these constraints, the central tendon is short, somehow behaving like a rigid rod, thus deteriorating the stiffness estimation derived from joint statics equilibrium. Therefore, it is necessary to investigate whether a data-driven compensator could effectively reduce the modeling errors.

Since the statics-equilibrium-based stiffness estimator suffers from undertrained behaviors of the central tendon, we intend to conduct stiffness control with feedback calibrated by data-driven compensation, that is, condition ②. First, we trained the data-driven compensator $h(\mathbf{L}, \mathbf{F}_t, \widehat{\mathbf{F}}_e)$. Given the tendon configuration $\mathbf{L}$, tendon tension $\mathbf{F}_t$, and estimated force $\widehat{\mathbf{F}}_e$, the learned mapping could output the force compensation $\widetilde{\mathbf{F}}_e$. Under the same periodic disturbances (Figure 8a), the stiffness control results are shown in Figure 8b. It is obvious that the errors under all the four targets are much smaller than those in condition ①, attributed to accurate feedback with the data-driven compensator. The overall control RMSE is only 0.0156 N/mm, which is reduced by 53.7% as compared with condition ①. It is worth noting that only the data set under *static* load tension was pre-trained offline, without samples under *dynamic* disturbances with varying joint stiffness, which would be sufficient already for reliable feedback calibration. Among the four targets, the marginal improvement can be observed under the minimal target stiffness (i.e., 0.28 N/mm). This is because compression of the spring connected to actuation tendons would be limited while only small tendon tension is applied, resulting in an insufficient compliant motion range after spring restoration. Consequently, as the bending angle increases, the tensegrity structure may collapse, unable to maintain both kinematics and statics equilibriums. As shown in Figure 8a, the force range under the average stiffness of 0.3499 N/mm would increase by 36.5%, as compared to 2.66 N under the average stiffness of 0.2569 N/mm. This indicates the potential for compensating human–robot collaborative ultrasound scanning tasks. A few limitations in the stiffness control could be discussed. For example, the control overshoot can still be observed (between 32 and 40 s) after feedback compensation, mainly due to the aforementioned lowered control bandwidth. To ensure reliable control in a wide stiffness range, advanced mechanisms/materials with promising controllable stiffness features will be explored in future studies.

To evaluate the closed-loop stiffness control performance in compliant manipulation, ultrasound scanning tests were conducted using either the tensegrity joint or rigid connection (Figure 9a,b). A piece of pork belly was selected as the subject. To generate dynamic disturbance, a balloon connected to a syringe was placed under the pork belly (Figure 9a), which could be manually inflated and deflated with 200 mL of air, thus generating up and down motions similar to respiration. Such motion was generated at a frequency of 0.25 Hz. Three scanning tests were performed: (RC) the ultrasound probe was rigidly connected to the UR5e manipulator, (OL) the probe was held by the tensegrity joint with open-loop stiffness control of 0.30 N/mm, and (CL) with closed-loop stiffness control (see Video SV1). The contact force was obtained after scanning by a film force sensor placed between the probe and the subject (RP-S5-ST, K-CUT, China). In test (RC), significant deformation of the subject would occur due to the unchanged probe position fixed by the manipulator, resulting in an increased contact force (max. 4.45 N) as shown in Figure 9c. In

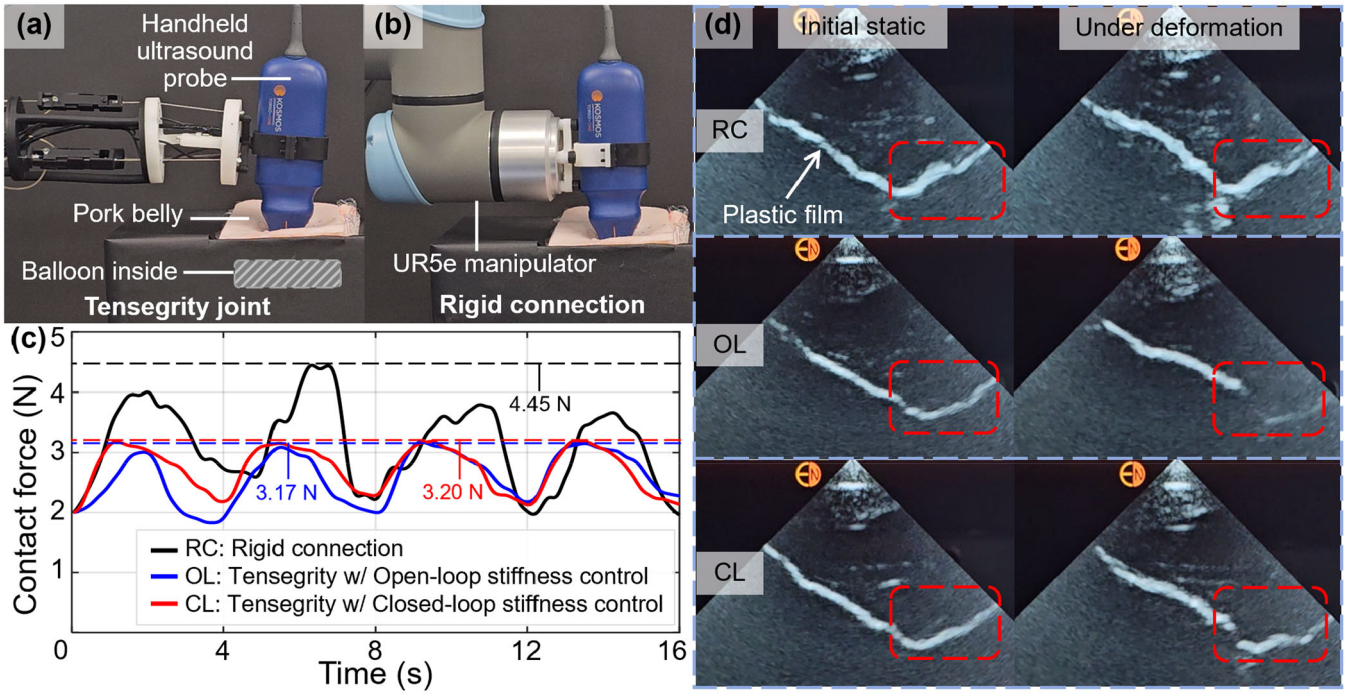

FIGURE 9 | Ultrasound scanning experiment with the tensegrity joint. (a) Experiment setup in which the ultrasound probe was held by the tensegrity joint. Dynamic disturbance of up and down motions was generated by a balloon connected to a syringe. (b) Experiment setup with the ultrasound probe rigidly connected to the manipulator. (c) Contact force between the probe and the subject during scanning. Three tests were conducted: (RC) the probe was rigidly connected to the manipulator, (OL) the probe was held by the tensegrity joint with open-loop stiffness control, and (CL) with closed-loop stiffness control, respectively. (d) Ultrasound image at the initial static condition and under deformation of the subject. [Color figure can be viewed at wileyonlinelibrary.com]

contrast, in tests (OL) and (CL), the contact force could be maintained at a lower level (< 3.20 N), attributed to the inherent structural compliance, providing gentle motion during the scanning and thus potentially avoiding causing pain to the patients. The ultrasound images are shown in Figure 9d, in which the plastic film (the bright region) could be regarded as the imaging target. In tests (RC) and (CL), a clear contour of the target could be seen in the image throughout the entire scanning process, despite the contact force increasing significantly in test (RC). The tensegrity joint failed to provide sufficient stiffness to maintain image quality in test (OL), due to the aforementioned uncertainties in the complex tensegrity modeling. However, the tensegrity joint with closed-loop stiffness control could maintain sufficient image quality while avoiding excessive contact force during the ultrasound scanning.

To further evaluate the inherent compliance of the tensegrity joint, compliance tests were also conducted. Both settings in Figure 9a,b were tested, in which impulsive disturbances were generated by rapidly inflating the balloon (< 0.2 s) with 200 mL of air (see Video SV1). The stiffness of the tensegrity joint was controlled to 0.30 N/mm, and the manipulator with rigid connection was set to built-in free-drive mode so that any external force would move the manipulator freely. The positions and contact force of the ultrasound probe were recorded by the EM tracking system and film force sensor, respectively, and are shown in Figure 10. In the setting with rigid connections, a large actuation force for motion acceleration was required due to the high inertia of the manipulator, leading to a significant delay in response to the impulsive disturbances. Such a delay results in a 43.5% increase in the peak contact force caused by the disturbance, compared to the 7.24 N

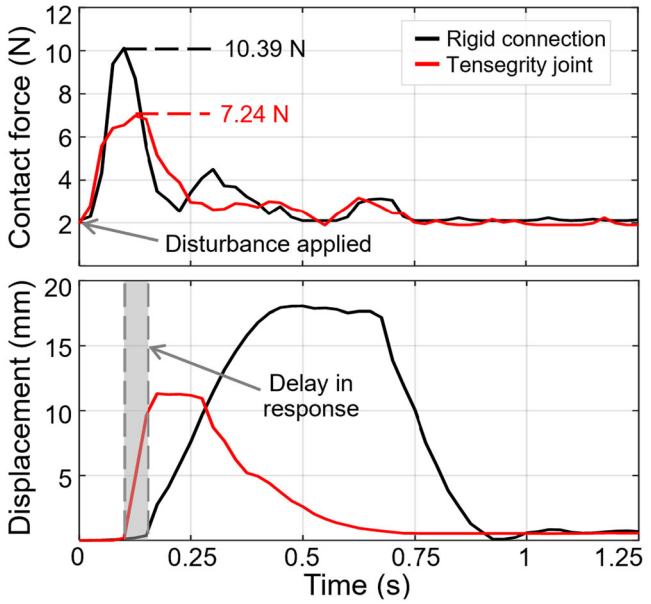

FIGURE 10 | Response to impulsive disturbances. With the settings in Figure 9a,b, impulsive disturbances were applied by rapidly inflating the balloon with 200 mL of air. The manipulator with rigid connection to the ultrasound probe was set to the built-in free-drive mode while the stiffness of tensegrity joint was closed-loop controlled at 0.30 N/mm. [Color figure can be viewed at wileyonlinelibrary.com]

force in the setting with the tensegrity joint. The inherent compliance and low inertia of the tensegrity could enable an immediate response to external disturbances, thus mitigating damage from inadvertent patient motion.

4 | Conclusion

In our previous work (Hao et al. 2024), we proposed a low-inertia 2-DOF tensegrity joint capable of precise motion control empowered by a learning-based controller, offering an alternative to traditional rotary joints. In particular for healthcare applications, such as robot-assisted ultrasound scanning, here we have enhanced the compliance of the fully constrained tensegrity joint. Our modified version seamlessly integrates with self-contained IMUs and tension sensors has been incorporated with a hybrid closed-loop stiffness controller, complementing the use of axial stiffness modulators along the tensegrity tendons. The synergistic hybrid utilization of model-based and data-driven stiffness estimators becomes the key to reducing various uncertainties in modeling the complex statics equilibrium typically found in the tensegrity.

In summary, we have developed a general stiffness control framework specific to the tensegrity joint for highly compliant robot tasks. Just using simple axial stiffness modulators comprising linear compression springs, the cutoff frequency of the robot joint operation can reach 11 Hz (Figure 5), outperforming that of our previous study (Hao et al. 2024). To validate the robustness of stiffness control for its specific use in robot-assisted ultrasound scanning, we presume the tensegrity joint would operate at almost 2 Hz during the robot active manipulation in appropriate response to patient physiological motion. Around 0.25-Hz periodic disturbance of the joint displacement (0–8 mm) is synthesized by a UR5e manipulator. With our framework, the force estimation compensator could reduce the stiffness control RMSE to 0.0156 N/mm, already by 53.7% (Figure 8b), relative to the situation when the stiffness feedback was only estimated from tensegrity statics without the compensator. The joint stiffness has been shown to be stably controlled close to the target reference within a low bandwidth. The ultrasound imaging quality could be maintained by closed-loop stiffness control while preventing excessive contact force. The inherent compliance and low inertia of the tensegrity joint allow for immediate response to external disturbances, thereby minimizing potential damage from inadvertent patient motion. If a higher range of bandwidth is required, a more responsive axial stiffness modulator (e.g., Chen and Sakovsky 2023; Levine et al. 2022) could be utilized, which features real-time stiffness adjustments and a broader range of joint stiffness. In our future work, considering the challenges of decoupling stiffness control, tendon management, and motion among the joints, we will explore the use and design of advanced controllers, such as data-driven model predictive control (Berberich et al. 2020; Piga et al. 2019), to handle the complexities of the dynamic model. To yield higher accuracy than least-squared regression as presented, Kolmogorov–Arnold Networks (KAN) (Liu et al. 2024) could serve as an alternative for estimating the direct mapping from tendon tension to joint stiffness.

Acknowledgments

This work is supported in part by the Research Grants Council of Hong Kong under Grant 17209021, 17210023, 17204124, STG1/E-401/23-N and C4026-21G; in part by the Multi-Scale Medical Robotics Center Ltd. funded by the Innovation and Technology Commission (ITC), Hong Kong; in part by the Guangdong Basic Research and Applied Basic Research Fund under Grant 2024A1515011509.

Conflicts of Interest

The authors declare no conflicts of interest.

Data Availability Statement

The authors have nothing to report.

References

Bel Hadj Ali, N., L. Rhode-Barbarigos, and I. F. C. Smith. 2011. "Analysis of Clustered Tensegrity Structures Using a Modified Dynamic Relaxation Algorithm." *International Journal of Solids and Structures* 48, no. 5: 637–647. https://doi.org/10.1016/j.ijsolstr.2010.10.029.

Berberich, J., J. Kohler, M. A. Muller, and F. Allgower. 2021. "Data-Driven Model Predictive Control With Stability and Robustness Guarantees." *IEEE Transactions on Automatic Control* 66, no. 4: 1702–1717. https://doi.org/10.1109/TAC.2020.3000182.

Chen, B., and H. Jiang. 2019. "Swimming Performance of a Tensegrity Robotic Fish." *Soft Robotics* 6, no. 4: 520–531. https://doi.org/10.1089/soro.2018.0079.

Chen, K. J., and M. Sakovsky. 2023. "Dynamically Reprogrammable Stiffness in Gecko-Inspired Laminated Structures." *Smart Materials and Structures* 33, no. 1: 015036. https://doi.org/10.1088/1361-665X/ad142d.

Chen, X., X. Zhang, Y. Huang, L. Cao, and J. Liu. 2022. "A Review of Soft Manipulator Research, Applications, and Opportunities." *Journal of Field Robotics* 39: 281–311. https://doi.org/10.1002/rob.22051.

Daemi, P., Y. Zhou, M. D. Naish, A. D. Price, and A. L. Trejos. 2023. "Development and Evaluation of a Friction Model for Tendon-Driven Soft Robotic Devices." *IEEE Transactions on Medical Robotics and Bionics* 5, no. 2: 429–441. https://doi.org/10.1109/tmrb.2023.3268755.

Diller, S. B., S. H. Collins, and C. Majidi. 2018. "The Effects of Electroadhesive Clutch Design Parameters on Performance Characteristics." *Journal of Intelligent Material Systems and Structures* 29, no. 19: 3804–3828. https://doi.org/10.1177/1045389x18799474.

Fang, G., X. Wang, K. Wang, et al. 2019. "Vision-Based Online Learning Kinematic Control for Soft Robots Using Local Gaussian Process Regression." *IEEE Robotics and Automation Letters* 4: 1194–1201. https://doi.org/10.1109/LRA.2019.2893691.

Fu, Y., W. Lin, X. Yu, J. J. Rodriguez-Andina, and H. Gao. 2023. "Robot-Assisted Teleoperation Ultrasound System Based on Fusion of Augmented Reality and Predictive Force." *IEEE Transactions on Industrial Electronics* 70: 7449–7456. https://doi.org/10.1109/TIE.2022.3201322.

Haddadin, S., A. De Luca, and A. Albu-Schaffer. 2017. "Robot Collisions: A Survey on Detection, Isolation, and Identification." *IEEE Transactions on Robotics* 33, no. 6: 1292–1312. https://doi.org/10.1109/tro.2017.2723903.

Hao, Y., X. Wang, X. Song, et al. 2024. "A Tensegrity Joint for Low-Inertia, Compact, and Compliant Soft Manipulators." *Advanced Intelligent Systems* 6, no. 2: 2300079. https://doi.org/10.1002/aisy.202300079.

Hinchet, R., and H. Shea. 2020. "High Force Density Textile Electrostatic Clutch." *Advanced Materials Technologies* 5, no. 4: 1900895. https://doi.org/10.1002/admt.201900895.

Hussain, I., A. Albalasie, M. I. Awad, et al. 2021. "Design and Control of a Discrete Variable Stiffness Actuator With Instant Stiffness Switch for Safe Human-Robot Interaction." *IEEE Access* 9: 118215–118231. https://doi.org/10.1109/access.2021.3105587.

Ipsen, S., D. Wulff, I. Kuhlemann, A. Schweikard, and F. Ernst. 2021. "Towards Automated Ultrasound Imaging-Robotic Image Acquisition in Liver and Prostate for Long-Term Motion Monitoring." *Physics in Medicine & Biology* 66: Article 094002. https://doi.org/10.1088/1361-6560/abf277.

Kim, U., C. Y. Maeng, G. Bak, and Y. J. Kim. 2022. "High-Stiffness Torque Sensor With a Strain Amplification Mechanism for Cooperative

Industrial Manipulators." *IEEE Transactions on Industrial Electronics* 69, no. 3: 3131–3141. https://doi.org/10.1109/tie.2021.3068656.

Le, H. M., T. N. Do, and S. J. Phee. 2016. "A Survey on Actuators-Driven Surgical Robots." *Sensors and Actuators, A: Physical* 247: 323–354. https://doi.org/10.1016/j.sna.2016.06.010.

Levine, D. J., G. M. Iyer, R. Daelan Roosa, K. T. Turner, and J. H. Pikul. 2022. "A Mechanics-Based Approach to Realize High-Force Capacity Electroadhesives for Robots." *Science Robotics* 7, no. 72: Article eabo2179. https://doi.org/10.1126/scirobotics.abo2179.

Li, W., X. Huang, L. Yan, H. Cheng, B. Liang, and W. Xu. 2024. "Force Sensing and Compliance Control for a Cable-Driven Redundant Manipulator." *IEEE/ASME Transactions on Mechatronics* 29, no. 1: 777–788. https://doi.org/10.1109/tmech.2023.3263922.

Li, W. Y., H. Nabae, G. Endo, and K. Suzumori. 2020. "New Soft Robot Hand Configuration With Combined Biotensegrity and Thin Artificial Muscle." *IEEE Robotics and Automation Letters* 5, no. 3: 4345–4351. https://doi.org/10.1109/lra.2020.2983668.

Lim, D., D. Kim, J. Park, and IEEE. 2021. Momentum Observer-Based Collision Detection Using LSTM for Model Uncertainty Learning. *IEEE International Conference on Robotics and Automation ICRA* [2021 IEEE International Conference on Robotics and Automation (ICRA 2021)]. IEEE International Conference on Robotics and Automation (ICRA), Xian, China.

Liu, Y., Q. Bi, and Y. Li. 2021. Development of a Bio-Inspired Soft Robotic Gripper Based on Tensegrity Structures. 2021 IEEE/RSJ International Conference on Intelligent Robots and Systems (IROS), Prague, Czech Republic.

Liu, Y., X. Dai, Z. Wang, et al. 2022. "A Tensegrity-Based Inchworm-Like Robot for Crawling in Pipes With Varying Diameters." *IEEE Robotics and Automation Letters* 7, no. 4: 11553–11560. https://doi.org/10.1109/LRA.2022.3203585.

Liu, Z., Y. Wang, S. Vaidya, et al. 2024. "Kan: Kolmogorov-arnold Networks." Preprint, arXiv, April 30. https://doi.org/10.48550/arXiv.2404.19756.

Luca, A. D., A. Albu-Schaffer, S. Haddadin, and G. Hirzinger. 2006. Collision Detection and Safe Reaction With the DLR-III Lightweight Manipulator Arm. 2006 IEEE/RSJ International Conference on Intelligent Robots and Systems.

Luca, A. d, and R. Mattone. 2005. Sensorless Robot Collision Detection and Hybrid Force/Motion Control. Proceedings of the 2005 IEEE International Conference on Robotics and Automation,.

Mak, C. H., Y. Li, K. Wang, et al. 2024. "Intelligent Shape Decoding of a Soft Optical Waveguide Sensor." *Advanced Intelligent Systems* 6: 2300082. https://doi.org/10.1002/aisy.202300082.

Mengacci, R., M. Garabini, G. Grioli, M. G. Catalano, and A. Bicchi. 2021. "Overcoming the Torque/Stiffness Range Tradeoff in Antagonistic Variable Stiffness Actuators." *IEEE/ASME Transactions on Mechatronics* 26, no. 6: 3186–3197. https://doi.org/10.1109/tmech.2021.3055364.

Oliveira, B., P. Morais, H. R. Torres, J. C. Fonseca, and J. L. Vilaça. 2024. "Design Optimization of Medical Robotic Systems Based on Task Performance Metrics: A Feasibility Study for Robotic Guided Vascular Laser Treatments." *Journal of Field Robotics* 41: 144–161. https://doi.org/10.1002/rob.22250.

Piga, D., M. Forgione, S. Formentin, and A. Bemporad. 2019. "Performance-Oriented Model Learning for Data-Driven MPC Design." *IEEE Control Systems Letters* 3, no. 3: 577–582.

Raina, D., H. Singh, S. K. Saha, et al. 2021. Comprehensive Telerobotic Ultrasound System for Abdominal Imaging: Development and In-Vivo Feasibility Study. 2021 International Symposium on Medical Robotics (ISMR).

Ramadoss, V., K. Sagar, M. S. Ikbal, J. H. L. Calles, R. Siddaraboina, and M. Zoppi. 2022. HEDRA: A Bio-Inspired Modular Tensegrity Robot With Polyhedral Parallel Modules. 2022 IEEE 5th International Conference on Soft Robotics (RoboSoft).

Sabelhaus, A. P., A. H. Li, K. A. Sover, et al. 2020. "Inverse Statics Optimization for Compound Tensegrity Robots." *IEEE Robotics and Automation Letters* 5, no. 3: 3982–3989. https://doi.org/10.1109/lra.2020.2983699.

Seok, D. Y., Y. B. Kim, S. Y. Lee, J. Kim, and H. R. Choi. 2020. "Ultra-Thin Joint Torque Sensor With Enhanced Sensitivity for Robotic Application." *IEEE Robotics and Automation Letters* 5, no. 4: 5873–5880. https://doi.org/10.1109/lra.2020.3010442.

Sun, Y., P. Tang, D. Dong, J. Zheng, X. Chen, and L. Bai. 2022. "Modeling and Experimental Evaluation of a Pneumatic Variable Stiffness Actuator." *IEEE/ASME Transactions on Mechatronics* 27, no. 5: 2462–2473. https://doi.org/10.1109/tmech.2021.3116871.

Thomas, G. P. L., T. D. Khokhlova, and V. A. Khokhlova. 2021. "Partial Respiratory Motion Compensation for Abdominal Extracorporeal Boiling Histotripsy Treatments With a Robotic Arm." *IEEE Transactions on Ultrasonics, Ferroelectrics, and Frequency Control* 68: 2861–2870. https://doi.org/10.1109/TUFFC.2021.3075938.

Ulrich, C., and L. N. S. Andreasen Struijk. 2021. "Probe Contact Forces During Obstetric Ultrasound Scans-A Design Parameter for Robot-Assisted Ultrasound." *International Journal of Industrial Ergonomics* 86: 103224.

Vespignani, M., J. M. Friesen, V. SunSpiral, and J. Bruce. 2018. Design of SUPERball v2, a Compliant Tensegrity Robot for Absorbing Large Impacts. 2018 IEEE/RSJ International Conference on Intelligent Robots and Systems (IROS).

Virga, S., O. Zettinig, M. Esposito, et al. 2016. Automatic Force-Compliant Robotic Ultrasound Screening of Abdominal Aortic Aneurysms. 2016 IEEE/RSJ International Conference on Intelligent Robots and Systems (IROS).

Wang, K., C.-H. Mak, J. D. L. Ho, et al. 2021. "Large-Scale Surface Shape Sensing With Learning-Based Computational Mechanics." *Advanced Intelligent Systems* 3, no. 11: 2100089. https://doi.org/10.1002/aisy.202100089.

Wang, K., X. Wang, J. D. L. Ho, et al. 2023. "A Fast Soft Robotic Laser Sweeping System Using Data-Driven Modeling Approach." *IEEE Transactions on Robotics* 39, no. 4: 3043–3058. https://doi.org/10.1109/TRO.2023.3262118.

Wang, X., J. Dai, H. S. Tong, et al. 2023. "Learning-Based Visual-Strain Fusion for Eye-in-Hand Continuum Robot Pose Estimation and Control." *IEEE Transactions on Robotics* 39, no. 3: 2448–2467. https://doi.org/10.1109/TRO.2023.3240556.

Wang, X., G. Fang, K. Wang, et al. 2020. "Eye-in-Hand Visual Servoing Enhanced With Sparse Strain Measurement for Soft Continuum Robots." *IEEE Robotics and Automation Letters* 5, no. 2: 2161–2168. https://doi.org/10.1109/LRA.2020.2969953.

Wolf, S., G. Grioli, O. Eiberger, et al. 2016. "Variable Stiffness Actuators: Review on Design and Components." *IEEE/ASME Transactions on Mechatronics* 21, no. 5: 2418–2430. https://doi.org/10.1109/tmech.2015.2501019.

Zappetti, D., Y. Sun, M. Gevers, S. Mintchev, and D. Floreano. 2022. "Dual Stiffness Tensegrity Platform for Resilient Robotics." *Advanced Intelligent Systems* 4, no. 7: 2200025. https://doi.org/10.1002/aisy.202200025.

Zhang, J., Y. Hu, Y. Li, et al. 2022. "Versatile Like a Seahorse Tail: A Bio-Inspired Programmable Continuum Robot For Conformal Grasping." *Advanced Intelligent Systems* 4, no. 11: 2200263. https://doi.org/10.1002/aisy.202200263.

Zhang, J., Z. Kan, Y. Li, Z. Wu, J. Wu, and H. Peng. 2022. "Novel Design of A Cable-Driven Continuum Robot With Multiple Motion Patterns." *IEEE Robotics and Automation Letters* 7, no. 3: 6163–6170. https://doi.org/10.1109/lra.2022.3166547.

Zhang, J. Y., and M. Ohsaki. 2006. "Adaptive Force Density Method for Form-Finding Problem of Tensegrity Structures." *International Journal of Solids and Structures* 43, no. 18–19: 5658–5673. https://doi.org/10.1016/j.ijsolstr.2005.10.011.

Supporting Information

Additional supporting information can be found online in the Supporting Information section.